Article

Toward the Ideal Organic Light-Emitting Diode. The Versatility and Utility of Interfacial Tailoring by Cross-Linked Siloxane Interlayers

Jonathan G. C. Veinot, and Tobin J. Marks

Acc. Chem. Res., **2005**, 38 (8), 632-643• DOI: 10.1021/ar030210r • Publication Date (Web): 10 June 2005

Acc. Chem. Res. **2005,** *38,* 632−643

Toward the Ideal Organic Light-Emitting Diode. The Versatility and Utility of Interfacial Tailoring by Cross-Linked Siloxane Interlayers

JONATHAN G. C. VEINOT† AND TOBIN J. MARKS*,‡

Department of Chemistry, University of Alberta, Edmonton, Alberta, Canada, T6G 2G2, and Department of Chemistry and the Materials Research Center, Northwestern University, Evanston, Illinois 60208

Received November 26, 2003

ABSTRACT

Small molecule and polymer organic light-emitting diodes (OLEDs) show promise of revolutionizing display technologies. Hence, these devices and the materials that render them functional are the focus of intense scientific and technological interest. The archetypical multilayer OLED heterostructure introduces numerous chemical and physical challenges to the development of efficient and robust devices. It is demonstrated here that robust, pinhole-free, conformal, adherent films with covalently interlinked structures are readily formed via self-assembling or spin-coating organosilane-functionalized molecular precursors at the anode−hole transport layer interface. In this manner, molecularly "engineered" hole transport and hydrocarbon anode functionalization layers can be introduced with thicknesses tunable from the angstrom to nanometer scale. These investigations unequivocally show that charge injection and continuity at the anode−hole transport layer interface, hence OLED durability and efficiency, can be substantially enhanced by these tailored layers.

Introduction

Chemistry and chemical principles have played a crucial role in the evolution of efficient organic light-emitting diodes (OLEDs). This is evident in the earliest observations of organic electroluminescence from anthracene single crystals,[1,2] through the pivotal discovery of efficient emission from amorphous small molecule-derived multilayer structures by Tang et al.[3] and from polymeric materials by Friend et al.[4] and culminating in current-generation device structures containing emissive triplet phosphors.[5] Until recently, chemical contributions have largely focused on tuning the wavelength, maximizing emission intensity, and controlling constituent physical properties such as solubility and volatility. As a result of extensive multidisciplinary efforts, modern OLEDs offer substantial benefits over conventional cathode ray tubes and liquid crystal displays and are predicted to revolutionize the display industry. OLEDs provide superior brightness and color purity, markedly lower drive voltages, as well as increased viewing angles. Despite these favorable attributes, significant chemical and physicochemical hurdles must be overcome to realize the full potential of OLEDs. These challenges include (1) effective mediation of charge carrier injection and, where necessary, charge carrier blocking, (2) thermal stability, and (3) operational lifetime. It will be seen that such issues reflect, among other factors, nanoscale interfacial phenomena in the OLED heterostructure that can be addressed/clarified by applying chemical assembly methodologies, as described in this Account.

How OLEDs Work

The basic multilayer structure of a prototypical OLED is shown in Figure 1A. Each layer plays a specific role in producing organic electroluminescence. Components include the transparent conducting oxide (TCO) anode, hole-transport layer (HTL), emissive layer (EML), electron-transport layer (ETL), and metallic low work function electrode (LWE) as the cathode. For the devices discussed here, the functions of the ETL and EML are satisfied by an aluminum quinoxalate (Alq) or poly(9,9-dioctylfluorene) (PFO) layer (Figure 2).

The basic mechanism of electroluminescence is now well-established. Under forward bias, the HTL is *oxidized* as holes are injected (electrons extracted) from the anode into its highest occupied molecular orbital (HOMO), and the ETL is *reduced* as electrons are injected from the cathode into its lowest unoccupied molecular orbital (LUMO). Charge carriers migrate under the applied electric field and recombine to form singlet and triplet excitons (bound excited-state electron−hole pairs) within

* To whom correspondence should be addressed. Telephone: (847) 491-5658. Fax: (847) 491-2990. E-mail: tjmarks@casbah.acns.nwu.edu.
† University of Alberta.
‡ Northwestern University.

Jonathan G. C. Veinot is an Assistant Professor at the University of Alberta (Edmonton, Canada). He received his Bachelor's degree in chemistry at the University of Western Ontario (London, Canada) in 1994. He subsequently carried out doctoral studies at York University (Toronto, Canada) while studying the chemical and electronic properties of cadmium sulfide nanoparticles, obtaining his Ph.D. in 1999. In 2000, Dr. Veinot was awarded an NSERC Post-Doctoral Fellowship, which was applied to his investigations of organic light-emitting diodes in the Marks group at Northwestern University (Evanston, IL). Dr. Veinot's current research program focuses on semiconductor and metal nanoparticles as well as transition-metal-based polymers whose applications include organic electronic devices such as OLEDs, TFTs, and photovoltaics.

Tobin J. Marks is the Vladimir N. Ipatieff Professor of Catalytic Chemistry and Professor of Materials Science and Engineering at Northwestern University. He received his B.S. from the University of Maryland (1966) and Ph.D. from Massachusetts Institute of Technology (1971). He received the ACS Award in Polymeric Materials, 1983; the ACS Award in Organometallic Chemistry, 1989; the ACS Award in Inorganic Chemistry, 1994; the ACS Award in the Chemistry of Materials, 2001; 1997 Centenary Medal, Royal Society of Chemistry; 2000 Chini Award, Italian Chemical Society; 2000 Cotton Medal, Texas A&M Section of the ACS; 2001 Willard Gibbs Medal, Chicago Section of the ACS; 2001 Burwell Award of the North American Catalysis Society; 2001 Linus Pauling Medal, Pacific Northwest ACS Sections; 2002 American Institute of Chemists Gold Medal; 2003 German Chemistry Society Karl Ziegler Medal; 2004 Royal Society of Chemistry Frankland Medal; Fellow, American Academy of Arts and Sciences, 1993; and Member, U. S. National Academy of Sciences, 1993. He has published 703 research articles and holds 65 U.S. patents. His current research interests include the synthesis and properties of organic and nanostructured electronic and optoelectronic materials, organometallic chemistry and catalysis, chemical vapor deposition, electronic ceramics, and polymer science.

10.1021/ar030210r CCC: $30.25
Published on Web 06/10/2005

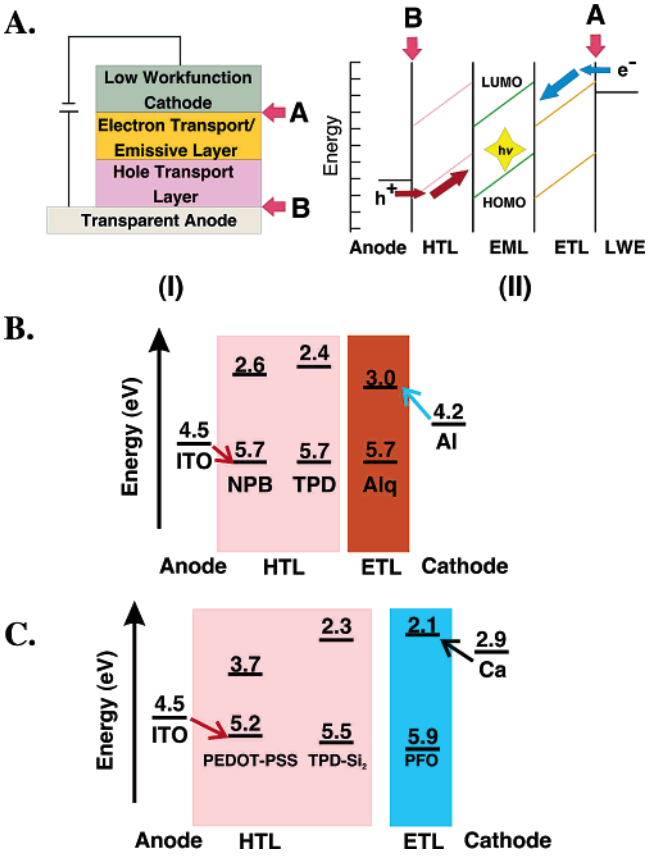

FIGURE 1. (A) (I) Schematic of atypical OLED heterostructure. (II) Energy level diagram of a typical multilayer OLED. LWE = low work function electrode, ETL/EL = electron transport/emissive layer, and HTL = hole transport layer. A and B indicate the cathode−ETL and anode−HTL interface, respectively. (B) Approximate energy diagram for electrodes and organic layers in the present OLEDs. Arrows denote the barriers to electron (blue) and hole (red) injection. (C) Approximate energy diagram for electrodes and organic layers in a typical PFO-based PLED. Arrows denote the barriers to electron (black) and hole (red) injection.

the EML. These excited-state species can return to the ground state via both radiative and nonradiative decay pathways. Energy level offsets of the anode and cathode work functions from the HTL HOMO and ETL LUMO energies, respectively, strongly influence the intrinsic carrier injection barriers.[6] From this abbreviated mechanistic description, one concludes that optimizing three electronic processes, (i) charge injection, (ii) transport, and (iii) recombination, will afford improved OLED performance. One successful approach to issue (iii) has been to maximize productive electron−hole recombination using dopants that emit from the triplet state. This strategy enhances quantum efficiency (photons produced/electrons injected, corrected for various geometric factors) by taking advantage of the 1:3 exciton singlet/triplet ratio predicted by simple spin statistics,[7] "triplet harvesting".[5] Other efforts to optimize OLED performance have focused on maximizing carrier transport and mobility via tailoring chemical structures. This has been a formidable challenge because the electronic properties of organic materials are typically characterized by preferential hole transport and low carrier mobilities. Hence, exciton formation is frequently limited by low electron fluence. This characteristic, combined with greater hole currents, significantly lowers OLED light output and external quantum efficiency.

The Importance of Interfaces

It is now generally accepted that carrier transport in most OLED heterostructures is largely injection-limited.[8] Hence, interfacial phenomena represent a challenging and important area of OLED science and technology and have been the subject of much recent theoretical and experimental investigation.[6,9−14] Because typical OLED carrier populations are electron-limited as noted above, most interfacial modification efforts have focused on hole injection/fluence attenuation and electron flux enhancement. Modifications have been applied to both cathode−organic and anode−organic interfaces, all influence charge injection and afford varying degrees of enhanced device response (e.g., in turn-on voltage, maximum luminance, and/or quantum efficiency). Notably, the exact interfacial structures and mechanistic roles remain incompletely defined.

Most approaches to cathode−ETL interface modification involve vapor-phase deposition. For representative vapor-deposited, anode/HTL [HTL = hole-transport layer = TPD (1,4-bis(phenyl-*m*-tolylamino)biphenyl) or NPB (1,4-bis(1-naphthylphenylamino)biphenyl)/Alq (tris(quinoxalinato)Al^{III})/cathode devices; Figure 2], dramatic increases in light output and quantum efficiency are observed upon insertion of angstrom-scale insulating layers (i.e., LiF,[15−20] CsF,[21] alkali metal acetates,[22] MgO,[20] Li_2O, NaCl, K_2O, RbCl, and KCl[23]) between the cathode and ETL. Explanations for these observations suggested largely in absence of definitive structural information include band bending,[24] tunneling injection,[20,22] LiF or CsF[21] dissociation from alkali metal halide reaction with cathode materials,[16] and/or depression of the Al surface potential,[16] which lowers the effective Al work function, as well as ETL protection during cathode deposition,[22,24] all consistent to some degree with mediation of the electron-injection barrier.

The anode−organic interface is more amenable to precision modification via solution- and vapor-phase techniques (e.g., thermal vapor deposition, reactive ion etching, and chemisorptive self-assembly), and numerous materials have been investigated, including layers of organic acids,[25−27] copper phthalocyanine,[28] dielectrics,[9,10] metals,[29] as well as polyaniline[27−29] and PEDOT−PSS (poly-3,4-ethylenedioxythiophene−polystyrene sulfonate).[29] As for cathode−ETL interfaces, the aforementioned anode−HTL interface modifications result in some performance enhancement. Diverse explanations for these effects include altering interfacial electric fields,[15,18,21−23,30,31] balancing electron/hole-injection fluence,[25,32] carrier confinement,[33] minimizing charge backscattering,[34] moderating anode−Fermi level−HTL HOMO energetic discontinuities,[25,35] and enhancement of injection via internal electric fields.[10] Unfortunately, the chemistry involved is generally

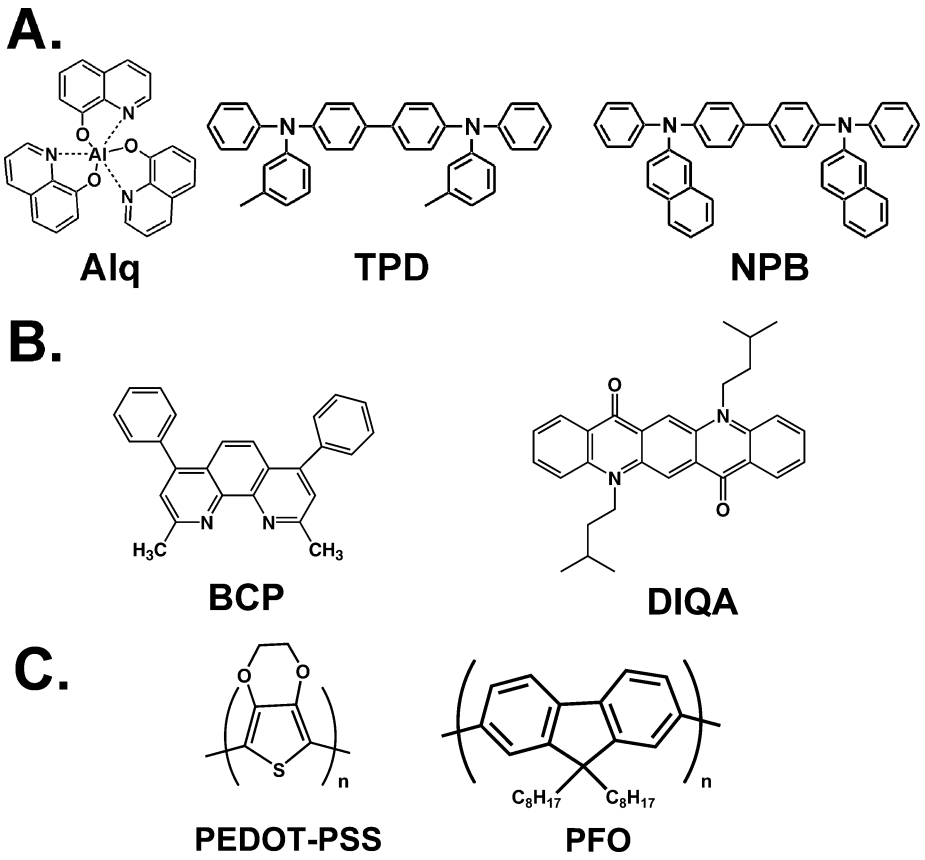

FIGURE 2. (A) Structural formulas of typical electron transport (Alq) and hole transport materials (TPD and NPB). (B) Exciton/hole blocking material BCP and emissive dopant DIQA. (C) Hole transport (PEDOT−PSS) and emissive (PFO) polymers.

not well-understood and lacks detailed characterization necessary to fully understand the origin of these effects. For these reasons, we were motivated to develop and understand chemistries capable of creating conformal, contiguous, nanoscopically well-defined, molecule-based anode−organic interfacial functionalization. It will be seen here that this can dramatically enhance OLED/PLED response and durability via understandable mechanisms.

Siloxane-Based Molecular Self-Assembly of Mono- and Multilayers

The great reactivity of chlorosilyl moieties toward surface hydroxyl functionalities such as those of indium−tin-oxide (ITO) surfaces makes siloxane-based self-assembly a versatile method for nanoscale tailoring of anode/HTL interfaces (Scheme 1).[9−14] The following discussion outlines methodologies for delivering mono- and multilayers of HTL adhesion-enhancing hole-transporting and insulating layers to the anode−organic interface and their effects on OLED response.

Triarylamine Layers for HTL Adhesion and Hole-Injection Control

Layer-by-layer, self-limiting chemisorptive self-assembly of triarylamine-organosilanes deposits ultrathin, transparent, covalently grafted hole-transport layers onto ITO anode surfaces for Alq-based OLEDs.[11−14] Scheme 1 depicts a general sequence for the $-SiCl_3$ reaction with

Scheme 1. (A) Mono- and (B) Multilayer Siloxane-Based Self-Assembly of ITO−HTL Interfacial Layers

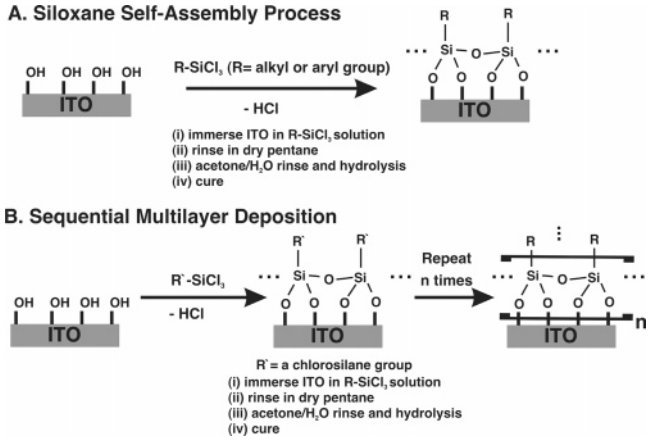

hydroxylated ITO surfaces. This self-limiting chemisorption yields chloride-free, conformal, nanoscale layers of organic thin films that are readily characterized using a diverse battery of physicochemical techniques (*vide infra*). When incorporated into archetypical OLED heterostructures, these molecule-scale layers have profound effects on luminous response.

A series of triarylamine hole-transporting SAM (self-assembled monolayer; Figure 3A) precursors designed to combine attributes of triarylamine hole transport and siloxane cross-linking were investigated for their influence on device response and thermal stability of archetypical vapor-deposited OLED heterostructures. When chemi-

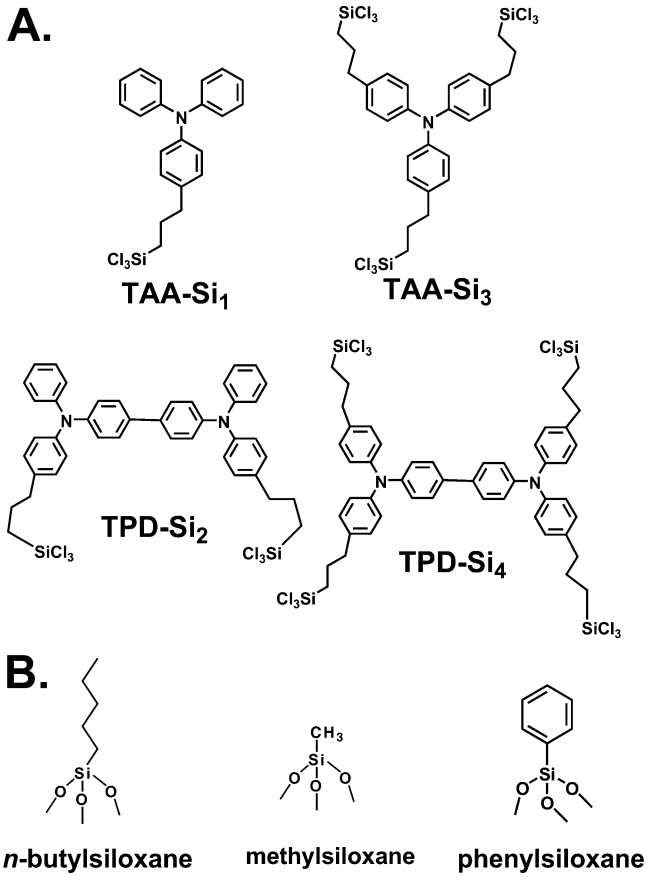

FIGURE 3. (A) $TAASi_1$, $TAASi_3$, $TPDSi_2$, and $TPDSi_4$, organic charge injection/adhesion layer precursors prior to chemisorption on ITO and cross-linking. (B) *n*-Butylsiloxane and methylsiloxane organic charge injection/adhesion materials shown after covalent attachment to ITO.

sorbed on ITO, these molecular units form monolayers of well-defined thickness (Table 1). For example, *bifunctional* $TPDSi_2$ affords an 18 Å thick monolayer (by X-ray reflectivity). UV−visible spectroscopy confirms that subsequent assembly cycles afford no additional film growth. In contrast, *trifunctional* $TAASi_3$ undergoes layer-by-layer deposition to build up cross-linked multilayers (Scheme 1). After each deposition, residual Si−Cl bonds within the $TAASi_3$ layer are readily hydrolyzed by exposure to "wet" acetone, and the self-assembly process was repeated to afford multilayers of precisely controlled thickness in 11.4 Å increments.

When the structural diversity of the molecularly engineered SAMs is combined with detailed physicochemical characterization, conclusions can be drawn regarding how interlayer chemical structure influences OLED response. Characterization results from AFM, advancing aqueous contact angles, optical spectroscopy, cyclic voltammetry, XPS, UPS, and X-ray reflectivity are summarized in Table 1. These analyses indicate that, in all cases, the self-limiting deposition process yields conformal, largely pinhole-free, hole-transporting molecule-scale layers of subnanometer dimensions. Incorporation into OLED heterostructures and evaluating the changes in device response reveals that the anode-bonded adsorbate molecule chemical structure dramatically influences ITO−organic interfacial integrity and charge injection characteristics as discussed below.

Anode−HTL Cohesion Effects

The known degradation of OLED response with thermal stress is poorly understood. It is conceivable that a primary failure mechanism arises from significant interfacial surface energy mismatches within the heterostructures, qualitatively indexed by advancing aqueous contact angle data. ITO has a disordered bixbyite crystal structure with a heavily hydroxylated surface (advancing aqueous contact angle of ∼0−30°).[36,37] In contrast, typical HTL materials (e.g., TPD and NPB) are hydrophobic with advancing aqueous contact angles of ∼90°. This large disparity in surface energies promotes the loss of anode−HTL interfacial integrity, particularly when the HTL materials are warmed near their glass transition temperatures (TPD T_g = 60 °C, and NPB T_g = 90 °C). For layered OLEDs (i.e., ITO/HTL/Alq/cathode), any loss of HTL physical contact will compromise hole-injection magnitude and uniformity, while the loss of HTL continuity may allow hole injection directly into the ETL, leading in the case of Alq to chemical degradation and erosion of emissive efficiency.[38]

$TAASi_1$, $TAASi_3$, $TPDSi_2$, and $TPDSi_4$ afford cross-linked mono- and multilayer networks well-suited for adhesion/injection interlayers at the ITO−HTL junction. These layers are covalently grafted to the ITO surface via siloxane linkages, making them physically robust, while the chemical similarities of the triarylamine structural units with the overlaying hole-transport materials (TPD and NPB) match MO energy levels while moderating surface energy mismatches. Resistance to thermal degredation is indicated by thermogravimetric analysis of cross-linked $TAASi_3$ and $TPDSi_2$ matrixes, which reveals only ∼5% weight loss on heating to 400 °C.

To evaluate relative OLED thermal stability with and without triarylamine-functionalized anodes, TPD and NPB films (50 nm) were vapor-deposited onto clean bare ITO and onto ITO coated with self-assembled/cross-linked $TAASi_3$ and $TPDSi_2$ SAMs. These model devices were then warmed above the HTL T_g values, and HTL morphology changes were assessed using electron and polarized optical microscopy. The microscopy clearly indicates that TPD and NPB undergo dewetting on unfunctionalized ITO surfaces (Figure 4), further confirmed by light element SEM/ESX maps indicating negligible C, H, or N in regions devoid of HTL "beads". Dewetting likewise occurs in bilayers having Alq overlayers, although somewhat more sluggishly. In contrast, when $TAASi_3$- and $TPDSi_2$-functionalized surfaces are employed, the HTL layers remain intact well above the HTL T_g, to 110 and 120 °C for TPD and NPB, respectively. Similar observations are obtained for $TAASi_1$ and $TPDSi_4$ SAMs. For comparison, the thermal response of the organosilane-buffered OLEDs was examined versus those containing the commonly employed vapor-deposited CuPc "buffer-layer".[11,12,32] Optical microscopy indicates that CuPc actually promotes crystal-

Table 1. Summarized Physical and Electronic Characteristics of Arylamine Layers Used as OLED Anodes

	TAA-Si_1	TAA-Si_3	TPD-Si_2	TPD-Si_4
λ_{max} (nm)	303	304	352	352
thickness (nm)[a]	1.2	1.4	1.8	1.6[b]
rms roughness (nm)[a]	0.4	0.7	0.7	1.3
advancing aqueous contact angle (deg)	90	87	90	90
$E_{p,a}/E_{p,c}$ (V)[c]	1.180/0.789	1.200/0.734	1.160/0.815	1.130/0.799
coverage Γ ($\times 10^{-10}$ mol/cm^2)[d]	4.5	4.2	2.5	2.1[e]
$\Delta E_{p,1/2}$ (mV)[f]	340	460	350	440
ionization potential (eV)[g]		5.8	6.1	

[a] From X-ray reflectivity of identical monolayers assembled on native oxide-coated Si(111). [b] Surface roughness introduces uncertainty in this value. [c] From cyclic voltammetry (CV) in a standard three-electrode cell and scan rate of 10 V/s. [d] Estimated from CV (0.1 V/s). [e] CV coverage consistent with XRR data assuming a two-electron redox process. [f] From CV, with a 0.1 V/s scan rate. $\Delta E_{p,1/2} > 90.6/n$ mV, indicating redox site interactions, site heterogeneity, or both. [g] From UPS analysis.

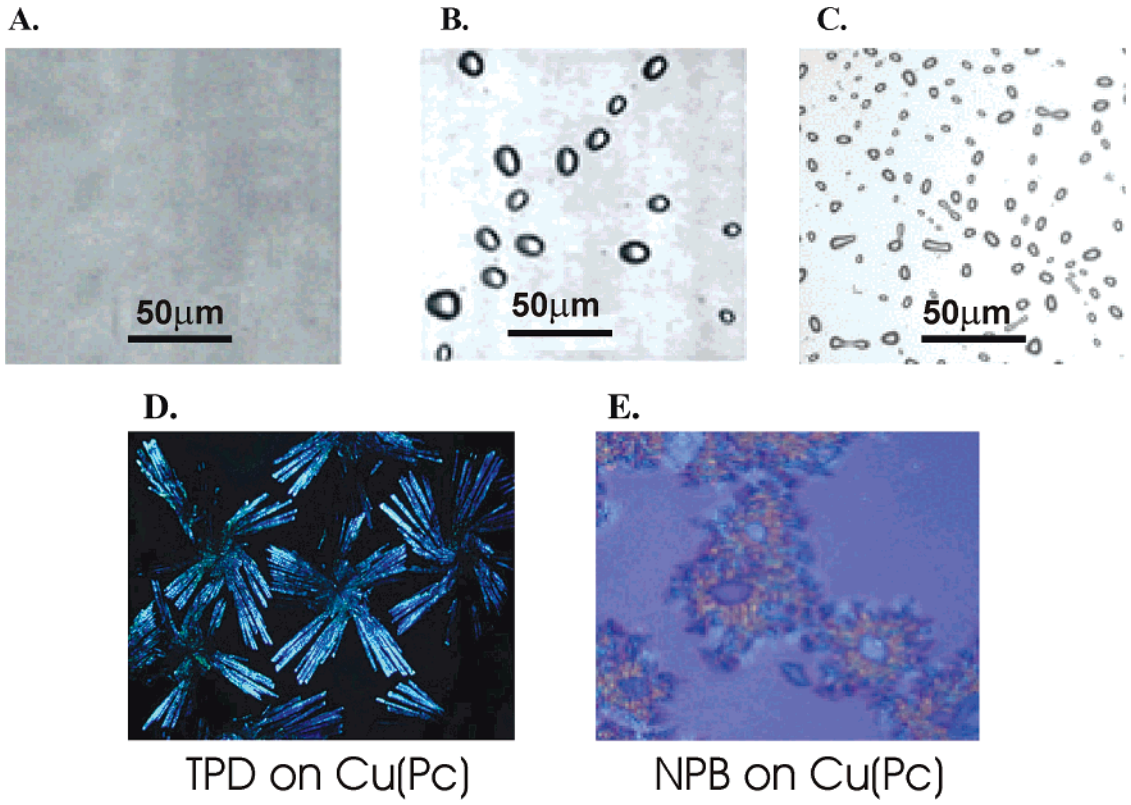

FIGURE 4. Optical micrographs of vapor-deposited HTL film (500 Å) morphology after annealing. (A) $TPDSi_2$ (80 °C for 1.0 h) on ITO substrates treated with a cured $TAASi_3$ SAM. (B) $TPDSi_2$ (80 °C for 1.0 h) on bare ITO. (C) NPB (120 °C for 1.0 h) on bare ITO. Spin-coated/cross-linked $TAASi_3$ and $TPDSi_2$ layers induce similar effects. Polarized optical microscopic images of 500 Å. TPD (D) and NPB (E) film morphologies following annealing the structure ITO/CuPc (100 Å)/HTL (500 Å) at 80 and 90 °C, respectively. Both images show templated crystallization of the HTL.

lization of the overlaying HTL materials upon warming (parts D and E of Figure 4), leading to poor anode−HTL contact and diminished response.

The aforementioned thermal stress results are readily related to OLED performance (Figure 5; for comparison, typical laptop display brightnesses are ~100 cd/m^2 and TV displays are ~200 cd/m^2). Irreversible luminance degradation of the bare ITO- and Cu(Pc)-based OLEDs upon heating at 95 °C can be associated with HTL decohesion and Cu(Pc)-promoted HTL crystallization. Both processes would disrupt multilayer integrity, decrease hole-injection efficiency, increase pinhole/defect formation, and allow degradative hole injection into the Alq EML.[38] In contrast, $TAASi_3$- and $TPDSi_2$-buffered devices exhibit a significantly enhanced response after heating (Figure 5), presumably a consequence of improved ITO/adhesion layer/HTL interfacial contact via reconstruction and interpenetration.[39] These experiments demonstrate that the covalently bonded $TPDSi_2$ and $TAASi_3$ interlayers significantly stabilize the anode−HTL interface, promote hole injection, as well as increase OLED light output and quantum efficiency. Qualitatively, all devices bearing adhesion/injection interfacial structures have greater resilience to avalanche breakdown, likely reflecting, among other factors, greater HTL adhesion.

Anode−HTL Carrier Injection

Another favorable aspect of the triarylamine-based SAMs is the capacity to support hole transport as suggested by

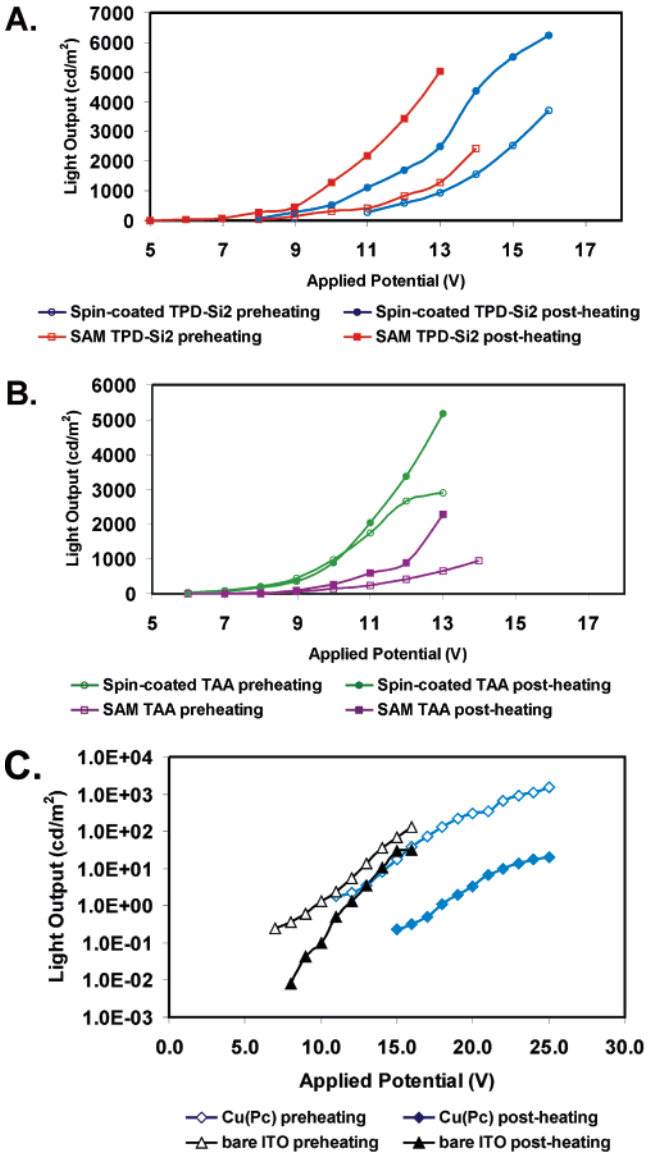

FIGURE 5. Effects of thermal stress (90 °C under vacuum) on the response characteristics of ITO/(injection/adhesion interlayer)/TPD (500 Å)/Alq (600 Å)/Al (1000 Å) OLED devices, where interlayer = (A) spin-coated $TPDSi_2$ (400 Å) and $TPDSi_2$ SAM (20 Å), (B) spin-coated $TAASi_3$ (150 Å) or SA-$TAASi_3$ $n = 4$ (~45 Å), and (C) ITO/[bare or 100 Å Cu(Pc)]/TPD (500 Å) /Alq (600 Å)/Al (1000 Å) OLED devices.

the aforementioned data and solution electrochemical experiments. ITO/SA-mono/multilayers are used as working electrodes.[11−14] Relative interfacial electron-transfer rates for strongly adsorbed redox-active sites such as the present SAMs can be qualitatively assessed by cyclic voltammetry.[40,41] Here, larger E_{ox}/E_{red} peak separations correspond qualitatively to slower heterogeneous charge transfer. Other factors contributing to E_{ox}/E_{red} peak separations include surface structural inhomogeneities, redox center−redox center interactions, and electrode−redox center distances.[42,43] In the present case, ITO/arylamine monolayer peak separations follow the trend $TPDSi_4$ < $TPDSi_2$ < $TAASi_1$ < $TAASi_3$, exactly the hole injection/efficiency measured by parallel solid-state "hole-only" devices[44] (here, a thin gold layer blocks electron

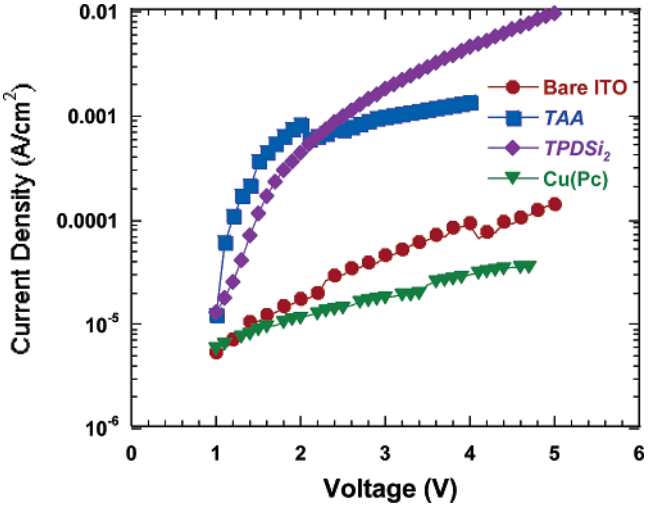

FIGURE 6. SAM dependence of hole-injection fluence in hole-only devices having the structure ITO/SAM/NPB (400 nm)/Au/Al.

injection, so that only hole currents are measured; *vide infra*).

Anodes functionalized with $TAASi_1$, $TAASi_3$, $TPDSi_2$, and $TPDSi_4$ SAMs all influence hole-only device and OLED response *similarly* versus bare ITO anodes and incisively probe interfacial chemical structural influence on device response. The hole-only devices (Figure 6) reveal a significant adsorbate structural dependence of hole-injection fluence as evidenced by the measured current densities. Here, hole-injection fluence varies by 1−2 orders of magnitude, with $TAASi_3$ < $TAASi_1$ < $TPDSi_2$ < $TAASi_4$ paralleling observed electroluminescence response trends in the corresponding OLEDs. At a bias of 10 V, archetypical OLEDs fabricated to maximize electron injection, ITO/(SAM)/NPB/tris-(8-hydroxyquinolato)aluminum (Alq):1% diisoamylquinacridone (DIQA)/2,9-dimethyl-4,7-diphenyl-1,10-phenanthroline (BCP, for hole, exciton blocking)/Li/AgMg, exhibit the following order of luminance: $TPDSi_4$ > $TPDSi_2$ > $TAASi_1$ > $TAASi_3$. The $TPDSi_4$-based device exhibits a maximum luminance of 70 000 cd/m² with a forward external quantum efficiency of 2.1%.[45]

One factor doubtlessly contributing to the enhanced performance noted above is also observed in devices using anodes coated with simple alkyl (e.g., *n*-butylsiloxane) SAMs, where effects of improved ITO−HTL contact via surface energy matching are also observed (*vide infra*).[46] More subtle structural differences differentiate $TPDSi_2$ and $TAASi_3$, where molecule-specific interactions with the overlying NPB HTL are evident in OLED response. For example, OLEDs with $TPDSi_2$ interlayers exhibit greater forward external quantum efficiencies (~0.8 versus 0.4% TAA SAM) and lower turn-on voltages (~8 versus 10 V) than analogous $TAASi_3$-based devices. These observations suggest stronger SAM−HTL affinity, better $\pi-\pi$ overlap, and more efficient hole hopping through the denser $TPDSi_2$ triarylamine network.

The consequences of using ITO anodes functionalized with self-assembled *multilayers* of triarylamine−organosilanes were extensively evaluated in Alq-based OLEDs. Introducing $TAASi_3$ multilayers [i.e., 1 (11.4 Å), 2 (23 Å), 4

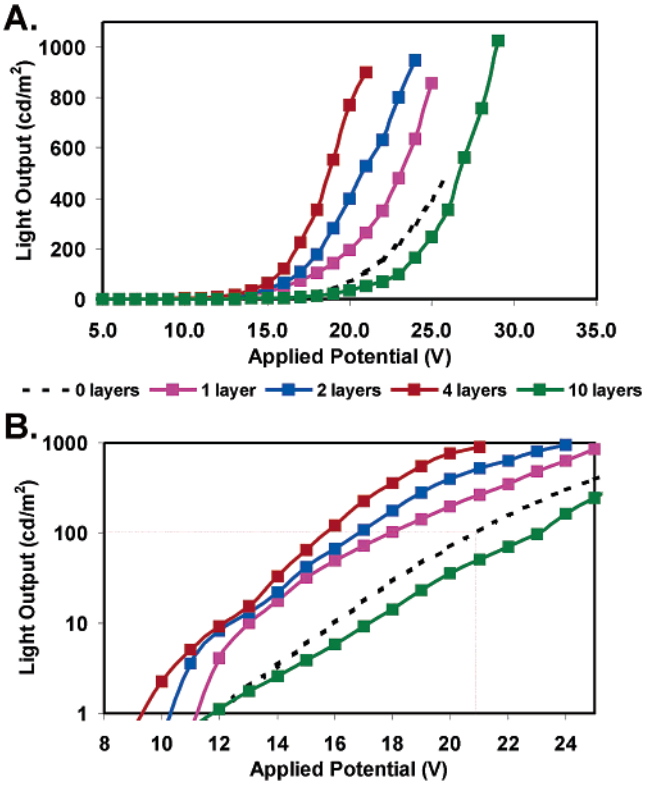

FIGURE 7. Dependence of device light emission on the number (n) of self-assembled TAA monolayers for OLEDs having the structure ITO/(SA-TAASi$_3$)$_n$/TPD (500 Å)/Alq (600 Å)/Al (1000 Å). (A) Light output versus bias voltage. (B) Expansion of the 5−15 V region.

(46 Å), and 10 (110 Å)] at the anode/HTL interface reveals that 1 → 2 → 4 layers results in a monotonic turn-on voltage decline (Figure 7), while devices with 10 self-assembled layers exhibit increased turn-on voltage, presumably reflecting the resistive nature of a thicker $TAASi_3$ matrix. The impact of $TAASi_3$ mono- and multilayer introduction is also evident in device external forward quantum efficiencies. An increase from 0.30% for bare ITO to 0.60% is observed for two $TAASi_3$ layers, versus a depression for thicker films (n = 10) to ~0.4%. The decreased quantum efficiency for thicker (n = 10) films parallels the trend in turn-on voltage, reflecting the resistive nature of the thicker $TAASi_3$ multilayer.

Hydrocarbon Monolayers—Contrasts with Conventional HTLs

In light of the nanoscale control afforded by conformal, chemisorptive self-assembly, Huang et al.[47] also investigated the effects of interlayer structural unsaturation on OLED response. They demonstrated that simple hydrocarbon SAMs of appropriate thicknesses (Figure 3B) can function analogously to conventional HTLs. Using chemisorptive self-assembly, ITO anodes were modified with $TAASi_3$, $TPDSi_2$, n-butylsiloxane, and methylsiloxane SAMs and evaluated as OLED anodes in ITO/SAM/Alq doped with DIQA BCP/Li/Al structures. Luminance versus voltage (L−V) and external quantum efficiency versus voltage characteristics are shown in Figure 8. It is not surprising, given the good hole-injection/transport characteristics of

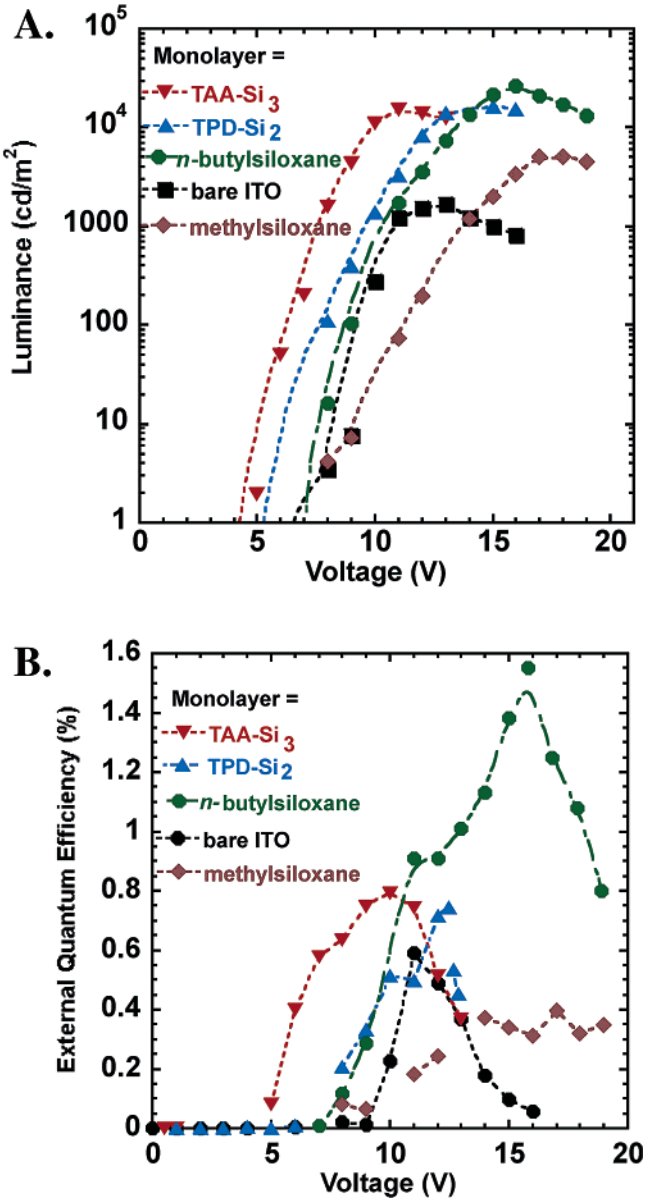

FIGURE 8. (A) Luminance versus voltage relationships for various SAMs used for anode functionalization in OLED devices of structure ITO/SAM/Alq doped with DIQA/BCP/Li/Al. (B) External quantum efficiency versus voltage relationships for the devices in A.

triarylamine-based structures, that a $TAASi_3$ or $TPDSi_2$ SAM HTL at the anode−EML/ETL interface leads to ~10× increase luminance efficiency relative to bare ITO (*vide supra*). These layers are also known to block efficiency-degrading electron transport to the anode and/or to minimize anode Fermi level−HTL energetic mismatches. These observations do not contradict established views on the role of HTLs but do demonstrate that HTL thickness can be reduced to ~1−2 nm and still retain favorable performance. However, in the traditional view of OLED function, replacement of $TAASi_3$ and $TPDSi_2$ with saturated hydrocarbon layers such as n-butylsiloxane should result in greatly diminished response. This is not the case. ITO/n-butylsiloxane SAM/Alq OLEDs exhibit efficiencies and luminance comparable to that of comparably configured $TAASi_3$ and $TPDSi_2$ SAM-based devices.

Typical device metrics for *n*-butylsiloxane-functionalized anode devices are impressive, with a maximum luminance of $\sim 2.6 \times 10^4$ cd/m^2 and a luminance per unit current density of ~5 cd/A at 15 V. However, alkyl-based interlayers either thinner or thicker than C4 yield diminished performance.

OLED response−anode modification models are diverse with HTL cohesion, clearly important as demonstrated above. However, existing models assume a conventional HTL and hence do not explicitly address the characteristics of OLEDs having structures such as saturated SAM-functionalized anodes. Interfacial electric fields should be relatively small in the absence of electron-donating or -withdrawing substituents in the SAM. Furthermore, the absence of triarylamine structural units precludes radical cation-mediated hole injection. Thus, the observed response more likely arises from reduced charge backscattering and improved charge injection balance. The image charge model describes charge injection at electrode−organic interfaces[48] and postulates that charges injected into organic matrixes induce countercharges at the electrode surface, which in turn exert a force on the injected charge. When the injected charge is proximate to the electrode surface ($\lesssim$1 nm), in the backscattering region, attractive Coulombic forces retard charge injection. Conversely, if the injected charge escapes this interfacial region, a lower barrier to injection results. X-ray reflectivity data indicate that the thickness of the *n*-butylsiloxane SAM (~6.2 Å) is comparable to typical charge backscattering regions (~1 nm).[45] For the image force model, if a hole is injected substantially through or beyond the backscattering region, hole injection will be enhanced, as appears to be the case for *n*-butylsiloxane-functionalized anodes, which exhibit improved response, versus unfunctionalized anodes. Further support for this model is provided by the decline in OLED performance when thinner methylsiloxane SAMs (~2.8 Å) are employed, even though they exhibit similar anode adhesion/wetting characteristics. The methylsiloxane layer has less than one-half the thickness of the *n*-butylsiloxane layer and the estimated ITO−HTL interfacial backscattering region. Unlike *n*-butylsiloxane, this SAM does not provide sufficient separation between injected and image charges to prevent backscattering; Coulombic forces attracting injected carriers back toward the anode hinder hole injection. In addition, greater defect densities associated with shorter alkyl chains[49] as in a methylsiloxane SAM should result in less efficient electron blocking and hole−electron recombination, thus limiting device efficiency. Nevertheless, the methylsiloxane-functionalized anode exhibits improved response versus bare ITO (Figure 8) likely reflecting, among other factors, improved surface energy matching with the HTL. It is generally accepted that hole and electron population balance is crucial for optimum OLED performance, with a traditional HTL role usually viewed as balancing hole−electron fluences for efficient recombination. Huang and co-workers demonstrated here that in absence of a traditional HTL structure, favorable hole−electron balance can still be achieved and reasonably efficient OLEDs fabricated.

Thicker Siloxane-Based HTLs

The facile solution processability of $TPDSi_2$ and $TAASi_3$ affords further versatility because these molecular precursors can also be deposited as nanoscale, cross-linked layers via spin coating. Thus, $TAASi_3$ and $TPDSi_2$ can be spin-coated onto ITO substrates from toluene solutions to yield robust conformal layers, following thermal annealing. The resulting layers are covalently grafted to the ITO surface and have thicknesses of ~15 and 40 nm, respectively, by profilometry. Devices with these thicker, cross-linked triarylamine interlayers exhibit superior device metrics to those having bare ITO anodes. Spin-coated $TPDSi_2$ layers afford by far the most efficient devices presented here. $TPDSi_2$ layers afford OLEDs with a maximum light output of ~15 000 cd/m^2 and a forward external quantum efficiency of 1.2%, dramatic improvements over bare ITO devices. Similar $TAASi_3$ devices show maximum luminance of ~3000 cd/m^2 and forward external quantum efficiency of 1.2%. Furthermore, the enhanced adhesion afforded by the corresponding SAMs remains, and thermal stressing OLED heterostructures with TPD HTLs actually enhance device performance, likely a result of improved cross-linking and decreased density of uncondensed Si−OH groups, which may chemically degrade Alq[50,51] and quench luminescence.[52,53] As is the case of molecular scale layers, the enhanced OLED performance is doubtless the result of several factors, including better anode−HTL adhesion, improved blocking of unproductive electron flow to the anode, planarization, and elimination of exciton-quenching sites.

Combining Anode Functionalization with Cathode−ETL Interfacial Tailoring

As noted above, electrode−organic interfacial tailoring has received considerable attention in efforts to optimize OLED performance. To date, most examples have focused on either the anode−HTL or cathode−ETL interface but not the combination. Huang et al. combined in a single device spin-coated $TPDSi_2$ interlayers with a known electron-injection enhancing hole/exciton-blocking layer, 2,9-dimethyl-4,7-diphenyl-1,10-phenathroline (BCP). Separately, both interlayers are known to enhance OLED response.[45,47] Various device structures were evaluated to investigate cooperativity effects of these performance-enhancing layers. Introduction of a $TPDSi_2$ interlayer into a ITO/NPB/Alq:DIQA/Li/MgAg heterostructure results in significant increases in current, a 50−80× improvement in light output, and increased forward external quantum efficiency (Figure 9). A similar $TPDSi_2$ interlayer effect is evident when ITO/NPB/Alq:DIQA/BCP/Li/MgAg and ITO/$TPDSi_2$/NPB/Alq:DIQA/BCP/Li/MgAg devices are compared. The significant increase in quantum and power efficiency arising from $TPDSi_2$ introduction argues that a greater density of injected holes accumulates at the HTL/ETL interface. Accumulated carriers at such interfaces alter

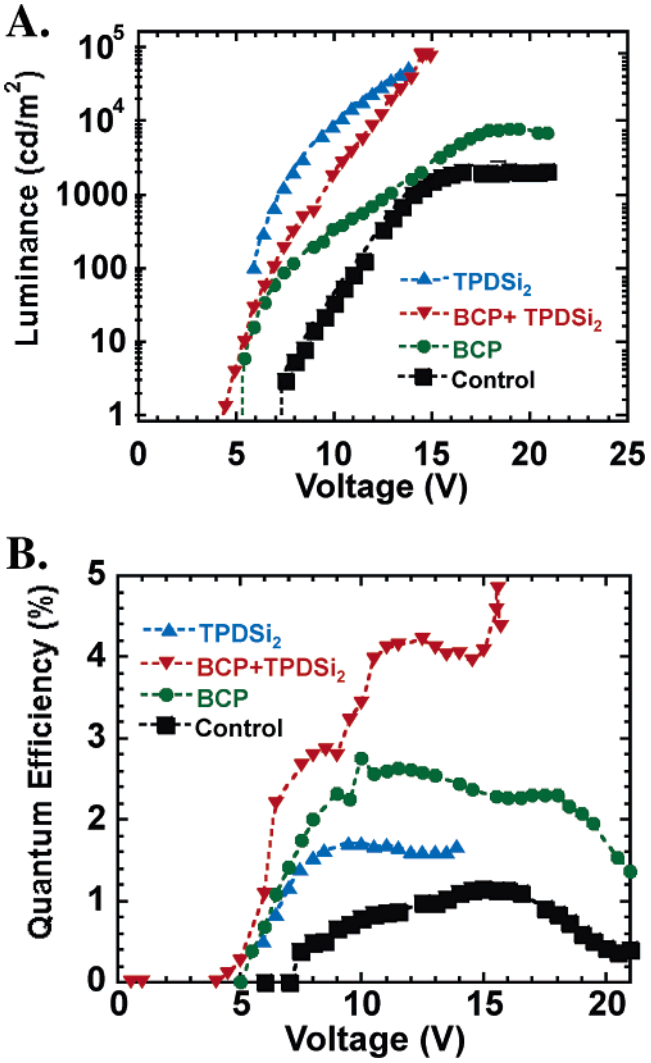

FIGURE 9. (A) Luminance−voltage characteristics for the OLED devices in Figure 1 having the structures: ITO/NPB/Alq:DIQA/Li/MgAg, ITO/TPDSi$_2$/NPB/Alq:DIQA/Li/MgAg, ITO/NPB/Alq:DIQA/BCP/Li/MgAg, and ITO/TPDSi$_2$/NPB/Alq:DIQA/BCP/Li/MgAg. (B) External quantum efficiency−voltage characteristics for OLED devices having the structures: ITO/NPB/Alq:DIQA/Li/MgAg, ITO/TPDSi$_2$/NPB/Alq:DIQA/Li/MgAg, ITO/NPB/Alq:DIQA/BCP/Li/MgAg, and ITO/TPDSi$_2$/NPB/Alq:DIQA/BCP/Li/MgAg. Lines through the data points are drawn as guides to the eye.

the internal electric fields within the OLED heterostructure and should enhance electron injection.[12,54] Li doping also enhances electron injection[46] and combined with the low work function Mg/Ag cathode should minimize electron−hole imbalance. The BCP layer, as noted before, functions as a hole/exciton-blocking layer[55,56] and enhances efficiency by confining electrons and excitons within the heterostructure emissive region. Note that OLEDs with BCP layers show significant performance enhancement over those without BCP layers (Figure 9).

When *both* TPDSi$_2$ and BCP interlayers are incorporated into the same device, all response metrics are enhanced. The external forward quantum efficiency is significantly increased (~4.5 versus 1.5% for TPDSi$_2$ alone versus 2.5% for BCP alone at 10−15 V bias) as is power efficiency (~16 versus ~8 Lm/W for TPDSi$_2$ alone versus ~10 Lm/W for BCP alone).[45,47] These results argue that the effects of enhanced hole injection and electron/exciton confinement are synergistic. Improving ITO−HTL contact with the TPDSi$_2$ interlayer affords increased hole currents, which in turn result in improved electron injection (*vide supra*). These greater carrier densities in the emissive region increase the probability of radiative recombination, hence device performance.

Triarylamine-Functionalized Anodes in Polymer Light-Emitting Diodes

Efficient polymer blue light-emitting diodes (PLEDs) are challenging to fabricate because suitable polymers must have large HOMO−LUMO gaps, hence large ionization potentials. This property renders hole injection at the anode−organic interface a limiting factor in device optimization. To date, this challenge has been addressed by placing polymeric hole transport layers between the ITO and emissive polymers. Colored, p-doped conductive polymers such as poly(3,4-ethylenedioxythiophene)−poly(styrenesulfonate) (PEDOT−PSS),[57,58] poly(pyrrole dodecylbenzene sulfonic acid) (Ppy-BDSA),[59] and poly(aniline camphorsulfonic acid) (PANI−CSA)[60] have been used. While increasing hole injection, their visible region absorption, corrosion of the ITO, and inability to address PLED thermal stability present major challenges. Alkyl siloxane SAMs have previously been used to enhance PLED lifetimes;[61] however, control of hole injection has not been acheived. The present triarylamine SAMs are transparent in the visible region while also offering enhanced hole injection and increased interfacial thermal stability in small molecule OLEDs. The fact that these interlayers might improve blue PLEDs prompted Yan et al. to fabricate blue PLED structures based on a poly(9,9-dioctylfluorene) (Figure 2) emissive layer, replacing the traditional polymeric HTL with a TPDSi$_2$ SAM.[62]

ITO/TPD-Si$_2$/PFO/Ca/Al PLED devices were fabricated, and the response compared to analogous PLEDs with ITO and ITO/PEDOT−PSS anodes. The electroluminescent spectra of the three devices are indistinguishable, identical to PFO photoluminescence. Figure 10 shows luminance−voltage, external quantum efficiency−voltage, and current−voltage response for all three device structures. Note that maximum external quantum efficiency and maximum luminance metrics are approximately 40% and 3× greater, respectively, for the TPDSi$_2$SAM-based device versus the PEDOT−PSS PLED. Note that because the maximum external quantum efficiency of the TPDSi$_2$SAM-based PLED occurs at somewhat higher bias, the maximum power efficiency exceeds the PEDOT−PSS system by only ~20%.

ITO/TPDSi$_2$ versus PEDOT−PSS/PFO/Au/Al hole-only device[41] response data provide valuable information regarding TPDSi$_2$ and hole injection at the anode−organic interface in PLED structures. Figure 11 shows that TPD-Si$_2$ SAMs enhance hole injection by nearly 100× compared to bare ITO. These results are paralleled by ultraviolet photoelectron spectroscopic (UPS) measure-

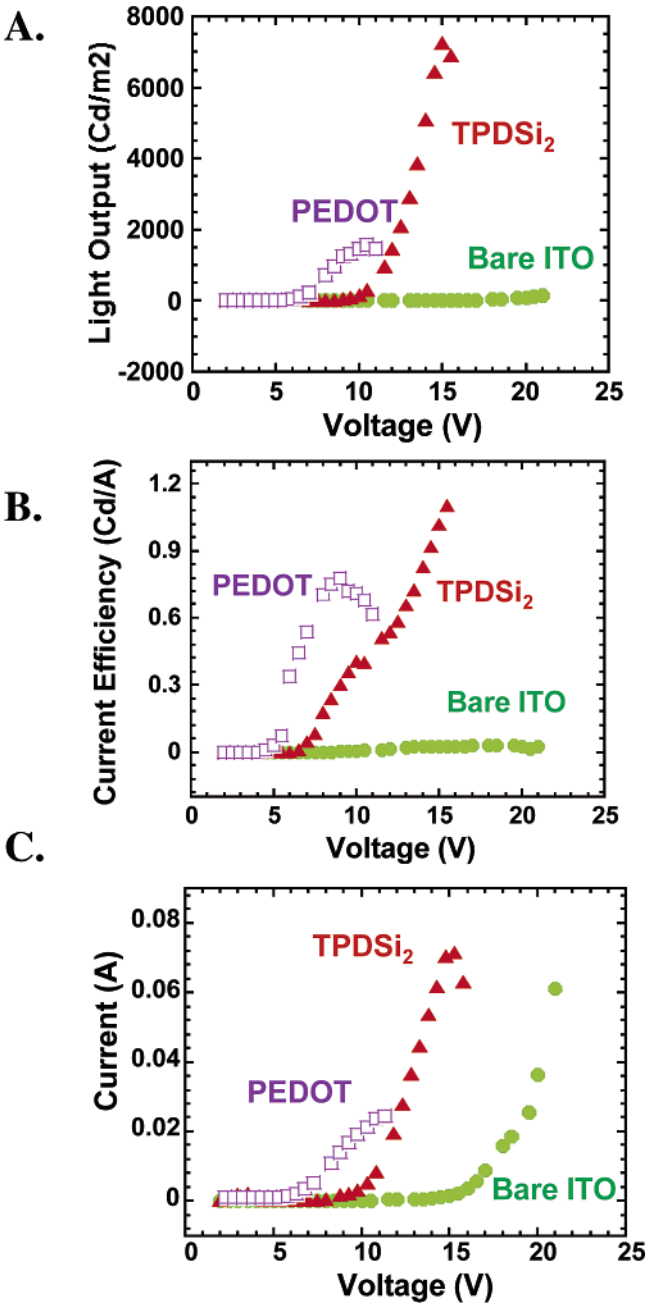

FIGURE 10. Efficacy of $TPDSi_2$ monolayers and PEDOT−PSS layers to improve PFO-based PLED response. (A) Light output. (B) Forward external quantum efficiency. (C) Current−voltage characteristics.

ments of the ionization potentials of bare ITO (~4.7 eV), PEDOT−PSS (~5.2 eV), and a TPD-Si_2 SAM (~5.5 eV). Because these data can be correlated with electrode work functions, note that the intrinsic hole-injection barrier from the ITO Fermi level to the PFO HOMO (~5.9 eV) is mediated by the $TPDSi_2$ SAM. When directly comparing the response of hole-only devices having PEDOT−PSS and TPD-Si_2 SAM anodes, note the lower hole current density for the polymer-modified anode. This suggests that the role of the $TPDSi_2$ monolayer differs from that of the polymer interlayer. Previously, Murata et al.[63] postulated that the hole-injection barrier at ITO/PEDOT−PSS interfaces was lowered by electron density build-up at the interface; hence, in a standard PLED model, PEDOT−PSS

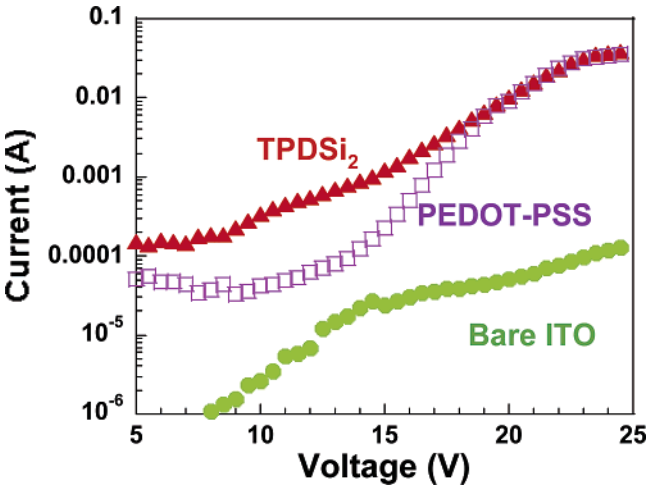

FIGURE 11. Efficacy of $TPDSi_2$ monolayers and PEDOT−PSS layers to improve hole-injection fluence in PFO-based hole-only devices.

acts as an electron-blocking layer. Clearly, this model must be supplemented by interfacial affinity effects as argued by advancing aqueous contact angles ($TPDSi_2$ ~ 80°, ITO/PEDOT−PSS ~ 30°, and PFO ~ 90°). Moreover, recent work shows in addition that $TPDSi_2$ SAMs and multilayers are far more effective hole injectors, more effective electron blockers, and less corrosive interlayers than PEDOT−PSS, with PLED current efficiencies as high as 17 cd/A achieved.[64,65] Furthermore, ITO alternatives such as Zn−In−Sn−O are more corrosion-resistant.[66]

Conclusions and Outlook

For organic light-emitting diodes to achieve ultimate performance hinges crucially on the numerous interfaces that influence heterostructure response. Recent work described herein to introduce well-defined, self-assembled mono- and multilayer structures at the anode−HTL interface demonstrates the possibility of moderating surface energy mismatches between hydrophilic ITO and overlying, hydrophobic, hole-transporting layers, adjusting carrier imbalances within the OLED structure, blocking undesired carriers from reaching electrodes, replacing traditional vapor-deposited HTLs, and providing a fundamental understanding of processes responsible for OLED device response. Triarylamine-based interfacial layers enhance HTL adhesion and thereby afford far greater hole-injection fluence, higher luminance, greater forward external quantum efficiency, and reduced turn-on voltage. OLEDs bearing $TPDSi_2$ anode adhesion/injection layers yield maximum luminance levels of 85 000 cd/m^2 and forward external quantum efficiencies of 4.5% in the absence of triplet dopants or low work function cathodes. Simple hydrocarbon interlayers also provide respectable responses. Thicker triarylamine layers have also been shown to replace traditional PLED HTL materials with significant success. An instructive feature is that beneficial hole-injecting properties can be combined with conventional hole/exciton blocking materials to produce highly efficient OLEDs. The structural diversity of siloxane-based self-assembly has provided insight into chemical

and physical processes governing OLED response and should be equally generalizable to PLEDs. The net results of such efforts in this and other laboratories will provide a deeper understanding of charge mobility and recombination in organic solids as well as completely new display technologies.

The authors wish to recognize the collaborative contributions of Drs. J. Malinsky, J. Cui, Q. Huang, and H. Yan. We also thank Professors N. Armstrong and M. Ratner and Dr. A. Burin for stimulating discussions. We thank the NSF-MRSEC program through the Northwestern Materials Research Center (DMR-0076097), the NSF (CHE-0201767), and the U.S. Display Consortium for support of this research. J. G. C. V. thanks NSERC of Canada for a postdoctoral fellowship.

References

(1) Helfirch, W.; Scheinder, W. G. Recombination radiation in anthracene crystals. *Phys. Rev. Lett.* **1965**, *14*, 229.
(2) Pope, M.; Kallmann, H. P.; Magnante, P. Electroluminescence in organic crystals. *J. Chem. Phys.* **1963**, *38*, 2042.
(3) van Slyke, S. A.; Tang, C. W. Organic electroluminescent diodes. *Appl. Phys. Lett.* **1987**, *51*, 913−915.
(4) Burroughes, J. H.; Bradley, D. C. C.; Brown, A. R.; Marks, R. N.; Mackay, K.; Friend, R. H.; Burns, P. L.; Holmes, A. B. Light-emitting-diodes based on conjugated polymers. *Nature* **1990**, *347*, 539−541.
(5) Baldo, M. A.; Thompson, M. E.; Forrest, S. R. High-efficiency fluorescent organic light-emitting devices using a phosphorescent sensitizer. *Nature* **2000**, *403*, 750−753.
(6) Ishii, H.; Sugiyama, K.; Ito, E.; Seki, K. Energy level alignment and interfacial electronic structures at organic metal and organic interfaces. *Adv. Mater.* **1999**, *11*, 605−625.
(7) Burin, A. L.; Ratner, M. A. Temperature and field dependence of the charge injection from metal electrodes into random organic media. *J. Phys. Chem. A* **2000**, *104*, 4704−4710.
(8) Baldo, M. A.; Forrest, S. R. Interface-limited injection in amorphous organic semiconductors. *Phys. Rev. B* **2001**, *64*, 85201.
(9) Malinsky, J. E.; Jabbour, G. E.; Shaheen, S. E.; Anderson, J. D.; Richter, A. G.; Armstrong, N. R.; Kipplelen, B.; Dutta, P.; Peyghambarian, N.; Marks, T. J. Self-assembly processes for organic LED electrode passivation and charge injection balance. *Adv. Mater.* **1999**, *11*, 227−231.
(10) Malinsky, J. E.; Veinot, J. G. C.; Jabbour, G. E.; Shaheen, S. E.; Anderson, J. D.; Lee, P.; Richter, A. G.; Burin, A. L.; Ratner, M. A.; Marks, T. J.; Armstrong, N. R.; Kipplen, B.; Dutta, P.; Peyghambarian, N. Nanometer-scale dielectric self-assembly process for anode modification in organic light-emitting diodes. Consequences for charge injection and enhanced luminous efficiency. *Chem. Mater.* **2002**, *14*, 3054−3065.
(11) Cui, J., Huang, Q.; Veinot, J. G. C.; Yan, H.; Wang, Q.; Hutchison, G. R.; Richter, A. G.; Evmenenko, G.; Dutta, P.; Marks, T. J. Anode interfacial engineering approaches to enhancing anode/hole transport layer interfacial stability and charge injection efficiency in organic light-emitting diodes. *Langmuir* **2002**, *18*, 9958−9970.
(12) Cui, J.; Huang, Q.; Veinot, J. G. C.; Yan, H.; Marks, T. J. Interfacial microstructure function in organic light-emitting diodes: Assembled tetraaryldiamine and copper phthalocyanine interlayers. *Adv. Mater.* **2002**, *14*, 565−569.
(13) Cui, J.; Huang, Q.; Wang, Q.; Marks, T. J. Nanoscale covalent self-assembly approach to enhancing anode/hole-transport layer interfacial stability and charge injection efficiency in organic light-emitting diodes. *Langmuir* **2001**, *17*, 2051−2054.
(14) Cui, J.; Wang, Q.; Marks, T. J. Covalent self-assembly approach to improvement of interfacial OLED anode/hole transport layer contacts. *Polymer Mater. Sci. Eng.* **2000**, *83*, 239−243.
(15) Jabbour, G. E.; Kawabe, Y.; Shaheen, S. E.; Wang, J. F.; Morrell, M. M.; Kippelen, B.; Peyghambarian, N. Highly efficient and bright organic electroluminescent devices with an aluminum cathode. *Appl. Phys. Lett.* **1997**, *71*, 1762−1764.
(16) Shaheen, S. E.; Jabbour, G. E.; Morell, M. M.; Kawabe, Y.; Kipplen, B.; Peyghambarian, N. Bright blue organic light-emitting diode with improved color purity using a LiF/Al cathode. *J. Appl. Phys.* **1998**, *84*, 2324−2327.
(17) Heil, H.; Steiger, J.; Karg, S.; Gastel, M.; Ortner, H.; Seggern, H. V.; Stobel, M. Mechanisms of injection enhancement in organic light-emitting diodes through an Al/LiF electrode. *J. Appl. Phys.* **2001**, *89*, 420−424.
(18) Mori, T.; Fujikawa, H.; Tokito, S.; Taga, Y. Electronic structure of 8-hydroxyquinoline aluminum/LiF/Al interface for organic electroluminescent device studied by ultraviolet photoelectron spectroscopy. *Appl. Phys. Lett.* **1998**, *73*, 2763−2765.
(19) Mason, M. G.; Tang, C. W.; Hung, L. S.; Raychaudhuri, P.; Madathil, J.; Giesen, D. J.; Yan, L.; Le, Q. T.; Gao, Y.; Lee, S. T.; Liao, L. S.; Cheng, L. F.; Salaneck, W. R.; Santos, D. A. d.; Gredas, J. L. Interfacial chemistry of Alq(3) and LiF with reactive metals. *J. Appl. Phys.* **2001**, *89*, 2756−2765.
(20) Huang, L. S.; Tang, C. W.; Mason, M. G. Enhanced electron injection in organic electroluminescence devices using an Al/LiF electrode. *Appl. Phys. Lett.* **1997**, *70*, 152−154.
(21) Piromreun, P.; Oh, H.-S.; Shen, Y.; Malliaras, G. G.; Scott, J. C.; Brock, P. Role of CsF on electron injection into a conjugated polymer. *Appl. Phys. Lett.* **2000**, *77*, 2403−2405.
(22) Ganzorig, C.; Suga, K.; Fujihira, M. Alkali metal acetates as effective electron injection layers for organic electroluminescent devices. *Mater. Sci. Eng.* **2001**, *B85*, 140−143.
(23) Wakimoto, T.; Fukuda, Y.; Nagayama, K.; Yokoi, A.; Nakada, H.; Tsuchida, M. Organic EL cells using alkaline metal compounds as electron injection materials. *IEEE Trans. Electron Devices* **1997**, *44*, 1245−1248.
(24) Schlaf, R.; Parkinson, B. A.; Lee, P. E.; Nebesny, K. W.; Jabbour, G.; Kippelen, B.; Peyghambarian, N.; Armstrong, N. R. Photoemission spectroscopy of LiF coated Al and Pt electrodes. *J. Appl. Phys.* **1998**, *84*, 6729−6736.
(25) Nüesch, F.; Forsythe, E. W.; Le, Q. T.; Gao, Y.; Rothberg, L. J. Importance of indium tin oxide surface acido basicity for charge injection into organic materials based light emitting diodes. *J. Appl. Phys.* **2000**, *87*, 7973−7980.
(26) Nüesch, F.; Kamarás, K.; Zuppiroli, L. Protonated metal-oxide electrodes for organic light emitting diodes. *Chem. Phys. Lett.* **1998**, *283*, 194−200.
(27) Appleyard, S. F. J.; Day, S. R.; Pickford, R. D.; Willis, M. R. Organic electroluminescent devices: Enhanced carrier injection using SAM derivatized ITO electrodes. *J. Mater. Chem.* **2000**, *10*, 169−174.
(28) van Slyke, S. A.; Chen, C. H.; Tang, C. W. Organic electroluminescent devices with improved stability. *Appl. Phys. Lett.* **1996**, *69*, 2160−2162.
(29) Shen, Y.; Jacobs, D. B.; Malliaras, G. G.; Koley, G.; Spencer, M. G.; Ioannidis, A. Modification of indium tin oxide for improved hole injection in organic light emitting diodes. *Adv. Mater.* **2001**, *13*, 1234−1238.
(30) Bliznyuk, V.; Ruhstaller, B.; Brock, P. J.; Scherf, U.; Carter, S. A. Self-assembled nanocomposite polymer light-emitting diodes with improved efficiency and luminance. *Adv. Mater.* **1999**, *11*, 1257−1261.
(31) Nüesch, F.; Rötzinger, F.; Si-Ahmed, L.; Zuppiroli, L. Chemical potential shifts at organic device electrodes induced by grafted monolayers. *Chem. Phys. Lett.* **1998**, *288*, 861−867.
(32) Forsythe, E. W.; Abkowitz, M. A.; Gao, Y. Tuning the carrier injection efficiency for organic light-emitting diodes. *J. Phys. Chem. B* **2000**, *104*, 3948−3952.
(33) Ho, P. K. H.; Granstrom, M.; Friend, R. H.; Greenham, N. C. Ultrathin self-assembled layers at the ITO interface to control charge injection and electroluminescence efficiency in polymer light-emitting diodes. *Adv. Mater.* **1998**, *10*, 769−774.
(34) Zuppiroli, L.; Si-Ahmed, L.; Kamars, K.; Nüesch, F.; Bussac, M. N.; Ades, D.; Siove, A.; Moons, E.; Grätzel, M. Self-assembled monolayers as interfaces for organic opto-electronic devices. *Eur. Phys. J. B* **1999**, *11*, 505−512.
(35) Lee, S. T.; Wang, Y. M.; Hou, X. Y.; Tang, C. W. Interfacial electronic structures in an organic light-emitting diode. *Appl. Phys. Lett.* **1998**, *74*, 670−672.
(36) Donley, C. L.; Dunphy, D. R.; Doherty, W. J.; Zangmeister, R. A. P.; Drager, A. S.; O'Brien, D. F.; Saavedra, S. S.; Armstrong, N. R. Indium−tin oxide organic interfaces. *ACS Sym. Ser.* **2003**, *844*, 133−153 and references therein.
(37) Kim, J. S.; Ho, P. K. H.; Thomas, D. S.; Friend, R. H.; Cacialli, F.; Bao, G. W.; Li, S. F. Y. X-ray photoelectron spectroscopy of surface-treated indium−tin oxide thin films. *Chem. Phys. Lett.* **1999**, *315*, 307−312.
(38) Aziz, H.; Popovic, Z. D.; NX, N. H.; Hor, A.; Xu, G. Degradation mechanism of small molecule-based organic light-emitting devices. *Science* **1999**, *283*, 1900−1902.
(39) For a non-OLED example, see: Kacker, N.; Kumar, S. K.; Allara, D. L. Wetting-induced reconstruction in molecular surfaces. *Langmuir* **1997**, *13*, 6366−6369.
(40) Finklea, H. O.; Liu, L.; Ravenscroft, M. S.; Punturi, S. Multiple electron tunneling paths across self-assembled monolayers of

alkanethiols with attached ruthenium(II/III) redox centers. *J. Phys. Chem.* **1996**, *100*, 18852−18858
(41) Weber, K.; Creager, S. E. Voltammetry of redox-active groups irreversibly adsorbed onto electrodes. Treatment using the Marcus relation between rate and overpotential. *Anal. Chem.* **1994**, *66*, 3164−3172.
(42) Zhang, W. W.; Ren, X. M.; Li, H. F.; Lu, C. S.; Hu, C. J.; Zhu, H. Z.; Meng, Q. J. Study on self-assembled monolayers of functionalized azobenzene thiols on gold: XPS, electrochemical properties, and surface-enhanced Raman spectroscopy. *J. Colloid Interface Sci.* **2002**, *255*, 150−157.
(43) Nielsen, M.; Larsen, N. B.; Gothelf, K. V. Electron-transfer reactions of self-assembled monolayers of thio(phenylacetylene)$_n$−Substituted chiral metal−salen complexes. *Langmuir* **2002**, *18*, 2795−2799.
(44) Ioannidis, A.; Forsythe, E.; Gao, Y. L.; Wu, M. W.; Conwell, E. M. Current−voltage characteristic of organic light emitting diodes. *Appl. Phys. Lett.* **1998**, *72*, 3038−3041.
(45) (a) Huang, Q.; Evmenenko, G.; Dutta, P.; Marks, T. J. Molecularly "engineered" anode adsorbates for probing OLED interfacial structure−charge injection/luminance relationships: Large, structure-dependent effects. *J. Am. Chem. Soc.* **2003**, *125*, 14704−14705. (b) Huang, Q.; Li, J.; Evmenenko, G. A.; Dutta, P.; Marks, T. J. Nanoscale "Engineered" Adsorbates To Probe Organic Light-Emitting Diode Interfacial Structure−Charge Injection−Luminance Relationships. Systematic Investigation of Large, Structurally Sensitive Effects. *J. Am. Chem. Soc.*, in press.
(46) Kawabe, Y.; Jabbour, G. E.; Shaheen, S. E.; Kippelen, B.; Peyghaambarian, N. A model for the current−voltage characteristics and the quantum efficiency of single-layer organic light emitting diodes. *Appl. Phys. Lett.* **1997**, *71*, 1290−1292.
(47) Huang, Q.; Cui, J.; Yan, H.; Veinot, J. G. C.; Marks, T. J. Small molecule organic light-emitting diodes can exhibit high performance without conventional hole transport layers. *Appl. Phys. Lett.* **2002**, *81*, 3528−3530.
(48) Lee, S. T.; Wang, Y. M.; Hou, X. Y.; Tang, C. W. Interfacial electronic structures in an organic light-emitting diode. *Appl. Phys. Lett.* **1998**, *74*, 670−672.
(49) Ohtake, T.; Mino, N.; Kazufumi, O. Effect of hydrocarbon chain length on arrangement of chemically adsorbed monolayers. *Langmuir* **1992**, *8*, 2081−2083.
(50) Liao, L. S.; He, J.; Zhou, X.; Lu, M.; Xiong, Z. H.; Deng, Z. B.; Hou, X. Y.; Lee, S. T. Bubble formation in organic light emitting diodes, *J. Appl. Phys.* **2000**, *88*, 2386−2390.
(51) Xu, M. S.; Xu, J. B.; Chen, H. Z.; Wang, M. Nanoscale investigation of moisture-induced degradation mechanisms of tris(8-hydroxyquinoline) aluminium-based organic light-emitting diodes. *J. Phys. D: Appl. Phys.* **2004**, *37*, 2618−2622.
(52) Yi, G. C.; Block, B. A.; Ford, G. M.; Wessels, B. W. Luminescence quenching in Er-doped $BaTiO_3$ thin films. *Appl. Phys. Lett.* **1998**, *73*, 1625−1627.
(53) Huignard, A.; Buissette, V.; Franville, A.-C.; Gacoin, T.; Boilot, J.-P. Emission processes in YVO_4:Eu nanoparticles. *J Phys. Chem. B* **2003**, *107*, 6754−6759.
(54) Parthasarathy, G.; Adachi, C.; Burrows, P. E.; Forrest, S. R. High-efficiency transparent organic light-emitting devices, *Appl. Phys. Lett.* **2000**, *76*, 2128−2130.
(55) Troadec, D.; Veriot, G.; Moliton, A. Blue light emitting diodes with bathocuproine layer. *Synth. Met.* **2002**, *127*, 165−168.
(56) Xie, Z. Y.; Hung, L. S.; Lee, S. T. High-efficiency red electroluminescence from a narrow recombination zone confined by an organic double heterostructure. *Appl. Phys. Lett.* **2001**, *79*, 1048−1050.
(57) Cao, Y.; Yu, G.; Zhang, C.; Menon, R.; Heeger, A. J. Polymer light-emitting diodes with polyethylene dioxythiophene−polystyrene sulfonate as the transparent anode. *Synth. Met.* **1997**, *87*, 171−174.
(58) Brown, T. M.; Kim, J. S.; Friend, R. H.; Caciallia, F.; Daik, R.; Feast, W. J. Built-in field electroabsorption spectroscopy of polymer light-emitting diodes incorporating a doped poly(3,4-ethylene dioxythiophene) hole injection layer. *Appl. Phys. Lett.* **1999**, *75*, 1679−1681.
(59) Gao, J.; Heeger, A. J.; Lee, J. Y.; Kim, C. Y. Soluble polypyrrole as the transparent anode in polymer light-emitting diodes. *Synth. Met.* **1996**, *82*, 221−223.
(60) Carter, S. A.; Angelopoulos, M.; Karg, S.; Brock, P. J.; Scott, J. C. Polymeric anodes for improved polymer light-emitting diode performance. *Appl. Phys. Lett.* **1997**, *70*, 2067−2069.
(61) Choi, B.; Rhee, J.; Lee, H. H. Tailoring of self-assembled monolayer for polymer light-emitting diodes. *Appl. Phys. Lett.* **2001**, *79*, 2109−2111.
(62) Yan, H.; Huang, Q.; Cui, J.; Veinot, J. G. C.; Kern, M. M.; Marks, T. J. High-brightness blue light-emitting polymer diodes via anode modification using a self-assembled monolayer. *Adv. Mater.* **2003**, *15*, 835−838.
(63) Murata, K.; Cina, S.; Greenham, N. C. Barriers to electron extraction in polymer light-emitting diodes. *Appl. Phys. Lett.* **2001**, *79*, 1193−1195.
(64) Yan, H.; Huang, Q.; Scott, B. J.; Marks, T. J. A polymer blend approach to fabricating the hole transport layer for polymer light-emitting diodes. *Appl. Phys. Lett.* **2004**, *84*, 3873−3875.
(65) Yan, H.; Lee, P.; Graham, A.; Armstrong, N. R.; Evmenenko, G. A.; Dutta, P.; Marks, T. J. High-performance hole transport layers for polymer light-emitting diodes. Implementation of organosiloxane crosslinking chemistry in polymeric electroluminescent devices. *J. Am. Chem. Soc.* **2005**, *127*, 3172−3183.
(66) Ni, J.; Yan, H.; Wang, A.; Yang, Y.; Stern, C. L.; Metz, A. W.; Jin, S.; Wang, L.; Marks, T. J.; Ireland, J.; Kannewurf, C. R. Synthesis and characterization of volatile zinc MOCVD precursors and their implementation in growth of highly transparent, conducting zinc- and tin-doped indium oxide anodes for polymer light-emitting diodes. *J. Am. Chem. Soc.*, ASAP.

AR030210R